Inorganic Chemistry

Article

pubs.acs.org/IC

Mg Intercalation in Layered and Spinel Host Crystal Structures for Mg Batteries

Alexandra Emly[†] and Anton Van der Ven*[,†,‡]

[†]Department of Materials Science & Engineering, University of Michigan, 2300 Hayward Street, Ann Arbor, Michigan 48109-2136, United States

[‡]Materials Department, University of California, Santa Barbara, California 93106-5050, United States

Supporting Information

ABSTRACT: We investigate electrochemical properties of Mg in layered and spinel intercalation compounds from first-principles using TiS_2 as a model system. Our calculations predict that Mg_xTiS_2 in both the layered and spinel crystal structures exhibits sloping voltage profiles with steps at stoichiometric compositions due to Mg-vacancy ordering. Mg ions are predicted to occupy the octahedral sites in both layered and spinel TiS_2 with diffusion mediated by hops between octahedral sites that pass through adjacent tetrahedral sites. Predicted migration barriers are substantially higher than typical Li-migration barriers in intercalation compounds. The migration barriers are shown to be very sensitive to lattice parameters of the host crystal structure. We also discuss the possible role of rehybridization between the transition metal and the anion in affecting migration barriers.

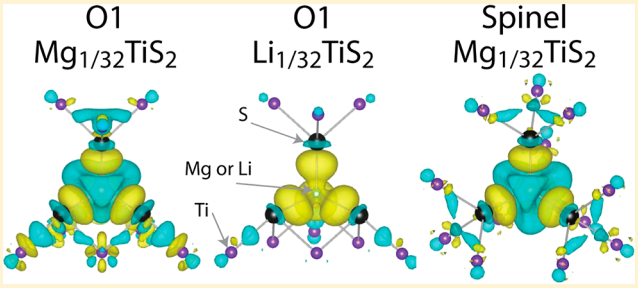

INTRODUCTION

Mg-ion batteries could be a promising alternative to Li-ion batteries because of the natural abundance of Mg, its lower cost, and the possibility of achieving increased capacity and energy density. One advantage of a Mg battery is the possible use of pure Mg as the anode as it is less susceptible to dendrite formation compared to Li-metal anodes.[1,2] However, while the properties associated with the intercalation of both Mg and Li ions into a variety of compounds were investigated in the 1990s,[3−6] only Li-ion battery technology has progressed significantly. Decades of fundamental and engineering research on Li-ion batteries have shown that a surprisingly large number of materials classes can react electrochemically with Li, offering a wide variety of chemistries to select from for the electrodes of Li-ion batteries.[7−9] This broad spectrum of candidate Li-electrode materials suggests that unexplored chemistries may also exist that can react with Mg electrochemically and that simultaneously overcome the low mobilities that typify Mg in crystalline solids. This possibility has spurred a renewed interest in Mg-ion batteries.[10,11] Many challenges remain, however, before Mg batteries become viable alternatives to Li-ion batteries. Not only are electrode materials with high Mg mobilities needed, but also new electrolyte chemistries are required that are chemically and electrochemically compatible with both Mg anodes and candidate cathode materials.[12,13]

There is currently a lack of fundamental insight as to the differences between Li-intercalation compounds and their Mg analogues. Although several experimental studies[14,5,15−17] have compared Mg-based electrodes to their Li counterparts, few computational studies have been reported.[18,19] The only structures found to exhibit moderate Mg diffusion to date are Chevrel phases.[20,21] While the atomistic mechanism of Mg diffusion in the Chevrel phases remains poorly understood, the presence of a cluster of transition metal atoms surrounding the Mg sites seems crucial to accommodate the more positive valence of Mg and facilitate high Mg mobilities. The Chevrel crystal structures, however, have little in common with typical Li-ion intercalation compounds. It is not clear, for example, whether Mg will intercalate within the layered or spinel host structures widely used in Li-ion batteries, and if they do, with which rates.

Here, we investigate the electronic, thermodynamic, and kinetic properties associated with the intercalation of Mg in layered and spinel host crystal structures from first-principles. There are many host chemistries that can be synthesized as having either the layered or spinel crystal structure. While the early cathodes of Li-ion batteries were based on transition metal sulfides (e.g., Li_xTiS_2), current technology relies on transition metal oxides as these exhibit substantially higher voltages with respect to a Li-metal anode. The early sulfides, however, exhibit exceptional kinetics and cycle lifetimes as cathodes in Li-ion batteries.[8,9] This is due to the high Li mobilities within the sulfide host structures as well as the absence of various, usually deleterious, phase transformations during Li removal and reinsertion. Furthermore, the electronic properties of sulfides are relatively simple, with electronic states remaining itinerant in the Li-composition intervals over which the electrodes are

Received: January 28, 2015
Published: April 23, 2015

DOI: 10.1021/acs.inorgchem.5b00188
Inorg. Chem. 2015, 54, 4394−4402

cycled. The transition metal oxides, in contrast, are more ionic, which affects ionic mobility and makes the host structure more susceptible to order/disorder and structural phase transformations as the Li content is varied. The electronic structures of transition metal oxides are also more complex, usually exhibiting localized states that can couple with local structural distortions (Jahn−Teller or polaronic states) and that may exhibit charge ordering and/or magnetic ordering as a function of Li concentration.[22,23]

Due to their excellent kinetic properties with respect to Li intercalation and their relatively simple electronic and phase transformation properties, the sulfides, in particular the TiS_2 chemistry, serve as useful model systems to explore the properties associated with Mg intercalation into layered and spinel crystal structures. Furthermore, the only compounds known so far to exhibit high Mg mobility are sulfur- and selenium-based Chevrel phases. The fact that TiS_2 exists in both the layered and spinel crystal structures makes this chemistry ideal to isolate the role of crystal structure on Mg-vacancy ordering tendencies and Mg diffusion.

METHODS

First-principles total energy calculations were performed with approximations to density functional theory (DFT) as implemented in the Vienna ab initio simulation package (VASP)[24,25] using projector augmented wave[26,27] pseudopotentials. Both the local density approximation (LDA) and generalized gradient approximation (GGA) as parametererized by Perdew, Burke, and Ernzerhof (PBE) were used. A large fraction of binding between adjacent TiS_2 slabs in the absence of intercalating species in the layered crystal structures is due to van der Waals attraction. Both LDA and GGA fail to account for van der Waals interactions. We therefore also applied van der Waals corrections with different exchange functionals using the vdW-DF[28,29] method: optPBE, optB86, and optB88. The valence configurations of the various pseudopotentials were the following: S $2s^2$, $2p^4$; Ti $3s^2$, $3p^6$, $4s^2$, $3d^2$; and Mg $2p^6$, $3s^2$. An energy cutoff of 420 eV was employed. Calculations were performed non-spin-polarized as we found that the inclusion of spin polarization has a negligible effect on formation energies and lattice parameters (these calculations can be found in Supporting Information). Migration barriers for Mg hops between adjacent interstitial sites were calculated using the nudged elastic band method[30] as implemented in VASP. Charge difference plots were calculated using PAW pseudopotentials having the $3s^2$ and $2s^1$ valence configurations for Mg and Li, respectively.

Cluster expansion methods,[31] as implemented in the CASM code,[32] were used to predict thermodynamic properties as a function of Mg concentration at room temperature. A cluster expansion as applied to Mg_xTiS_2 describes the dependence of the fully relaxed energy of the crystal as a function of the degree of order among the Mg ions and vacancies occupying the interstitial sites of TiS_2. The basis functions of a cluster expansion are polynomials of occupation variables σ_l belonging to clusters of interstitial sites,[31] with σ_l equal to 1 when Mg occupies site l and 0 when it is vacant. A cluster expansion can be used to extrapolate first-principles total energies of a subset of Mg-vacancy arrangements to any Mg-vacancy arrangement within Monte Carlo simulations. The expansion coefficients of truncated cluster expansion Hamiltonians were fit to first-principles formation energies.[33] The cluster expansions were then subjected to grand canonical Monte Carlo simulations to study finite-temperature thermodynamic properties as a function of Mg composition x in Mg_xTiS_2 ($0 \le x \le 0.5$) in both the spinel crystal structure and the most stable layered form.

To assess the reliability of the various approximations to DFT in describing the properties of Mg_xTiS_2, we compare in Figure 1 the a- and c-lattice parameters as a function of Mg concentration for the lowest energy Mg-vacancy orderings within the intercalation layers of the layered form of TiS_2 having an ABAB sulfur stacking sequence.

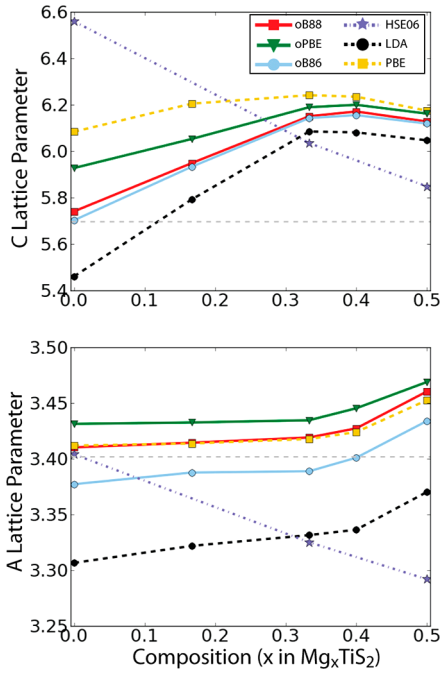

Figure 1. Calculated c- and a-lattice parameters for Mg_xTiS_2 ($0 < x < 0.5$) using different approximations to DFT. Solid lines correspond to PBE with vdW-DF corrections to account for van der Waals attraction. Dashed lines correspond to LDA (black) and standard PBE (yellow) while the purple dot−dashed line corresponds to HSE06.

Since migration barriers are very sensitive to the c-lattice parameter in layered intercalation compounds,[32,34] it is essential that the correct dependence of this lattice parameter with concentration is predicted. Many layered intercalation compounds undergo a contraction of the c-lattice parameter as the concentration of intercalating species decreases. This can be attributed to a combination of increased covalency of the host[35] and a reduction of steric hindrance upon extraction of intercalating species. Figure 1 and past studies[32] show that LDA, while correctly predicting a contraction of the c-lattice parameter as the number of intercalating species between the layered TiS_2 slabs decreases, has a tendency to overbind and quantitatively underpredicts the c-lattice parameter of TiS_2. Nevertheless, LDA has proven very reliable in predicting qualitative trends in layered intercalation compounds, including Li_xTiS_2[32] and Li_xCoO_2.[35] GGA in contrast predicts a c-lattice parameter for TiS_2 that is substantially above the experimental value. HSE has so far also not proven reliable in accounting for van der Waals interactions[36] and predicts an increase in the c-lattice parameter as the Mg concentration decreases with a c-lattice parameter of TiS_2 that differs from the experimental value by 15%. As is clear in Figure 1, the application of van der Waals corrections to GGA based on the vdW-DF[28,29] method, such as optPBE, optB86, and optB88, results in more accurate predictions of the c-lattice parameter as compared to those predicted with LDA and GGA.

Due to the accuracy of optB86 in predicting the c-lattice parameter of TiS_2 we only report results calculated with this approximation. Nevertheless, similar calculations were performed with optB88 and LDA, and results using these approximations can be found in Supporting Information. We found that all three approximations (optB86, optB88, and LDA) predict the same qualitative trends.

RESULTS

Phase Stability. We explored the relative phase stability of four layered forms of Mg_xTiS_2 as well as that of the spinel form (all five shown in Figure 2) of Mg_xTiS_2 as a function of Mg concentration. The four layered forms of Mg_xTiS_2 have different stacking sequences of the TiS_2 slabs. Each TiS_2 slab

DOI: 10.1021/acs.inorgchem.5b00188
Inorg. Chem. 2015, 54, 4394−4402

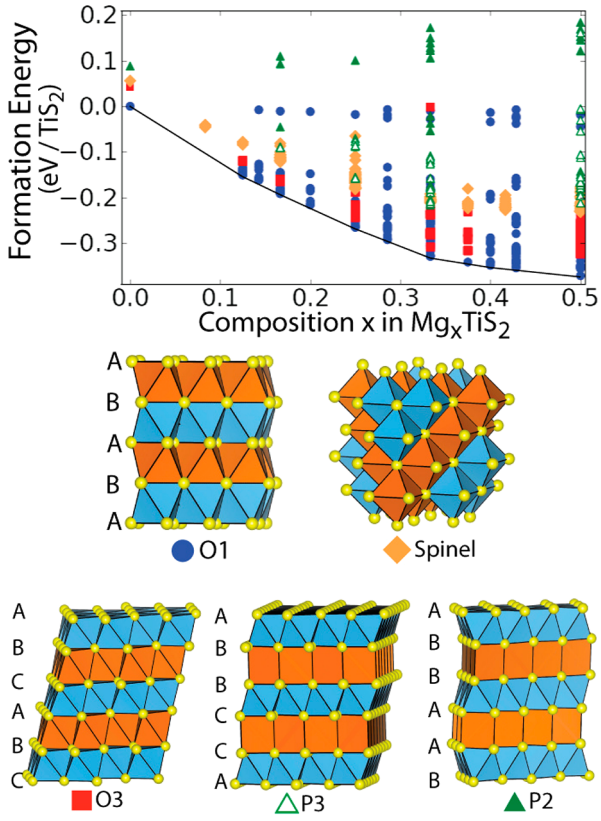

Figure 2. Calculated formation energies for different Mg-vacancy orderings within the spinel and various layered forms of Mg_xTiS_2. The O1 structure is the most stable across the entire composition range.

consists of an AB stacking of close-packed two-dimensional triangular lattices of sulfur. The Ti atoms occupy octahedrally coordinated interstitial sites between the sulfur planes. As candidate layered host structures, we considered O1, O3, P3, and P2, using the nomenclature introduced by Delmas et al.[37] $LiTiS_2$ is stable in the O1 host (having an ABAB stacking sequences of close-packed sulfur layers) and maintains that host structure during deintercalation.[8,9,32] O3 (having an ABCABC stacking sequence of sulfur planes) is a common host of layered lithium−transition metal oxides such as Li_xCoO_2 and $Li_x(Ni_{1/3}Mn_{1/3}Co_{1/3})O_2$ while P3 (ABBCCA) and P2 (ABBA), which have trigonal prismatic sites in the intercalation layers, are common among many Na-intercalation compounds. Only O3 and P3 can be formed from O1 through a shuffle of the TiS_2 slabs relative to each other.

We calculated the energies of 212 symmetrically distinct Mg-vacancy configurations over the octahedral sites of the O1 form of TiS_2, 300 configurations over the octahedral sites of the O3 host, and 75 and 34 configurations over the prismatic sites of the P3 and P2 host structures, respectively. We also calculated the energies of 169 Mg-vacancy configurations over the octahedral sites of the spinel form of TiS_2. Similar to Li, we found that Mg prefers octahedral sites to the tetrahedral sites in O1, O3, and the spinel form of TiS_2.

Figure 2 shows the calculated formation energies of all the Mg-vacancy configurations considered within the five host structures of Mg_xTiS_2 ($0 \le x \le 0.5$). The O1 form of Mg_xTiS_2 has the lowest formation energy for all values of x between 0 and 0.5. The other layered host structures, while less stable than O1, on the whole have lower formation energies than the spinel form of $MgTiS_2$. The prediction that O1 is the most stable host for all Mg concentrations suggests that bonding within Mg_xTiS_2 is very similar to that in Li_xTiS_2. The P3 and P2 hosts tend be stable when intercalated with large species such as Na. The ionic radius of Mg^{2+} is similar to that of Li^+ and smaller than that of Na^+. The O3 host is stable in the transition metal oxides, which tend to be more ionic than the transition metal sulfides. The O1 crystal structure is isomorphic to that of CdI_2, which is characterized by covalent bonding, while the O3 crystal structure is isomorphic to that of $CdCl_2$, which has a more ionic character.

Mg Ordering in Layered Mg_xTiS_2. A variety of ordered phases are predicted to be stable at intermediate Mg concentrations in the O1 host structure. These ordered phases have formation energies that reside on the convex hull in Figure 2a. While ground states are predicted at six different concentrations, three are especially stable in wide Mg-chemical-potential ranges. One stable ordered phase is $Mg_{1/6}TiS_2$ in which every other layer of Mg sites is completely empty while the remaining alternating layers are one-third filled (Figure 3). This staging predicted for Mg_xTiS_2 is similar to that

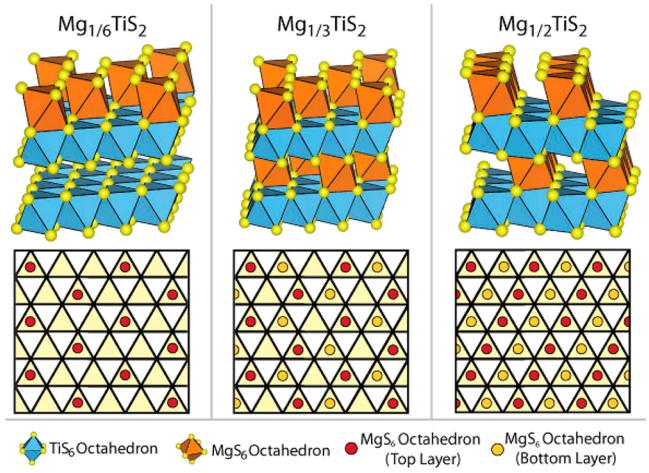

Figure 3. Mg in-plane ordering in the three ground states of O1 Mg_xTiS_2 ($0 \le x \le 0.5$) along with projections of the Mg ordering within the intercalation layers. Yellow triangles denote potential octahedral Mg sites. Red circles correspond to Mg ions in one layer while yellow circles denote Mg atoms occupying the adjacent layer. Sulfur atoms occupy the vertices of each triangle. The white triangles denote tetrahedral sites.

in graphite,[38] $LiTiS_2$,[39] and $LiCoO_2$.[40,41] Another stable ground state is $Mg_{1/3}TiS_2$ in which every layer has one-third filling. The Mg ions order in a $\sqrt{3}a \times \sqrt{3}a$ supercell within the filled layers of $Mg_{1/6}TiS_2$ and $Mg_{1/3}TiS_2$. This in-plane ordering changes to row ordering in $Mg_{1/2}TiS_2$ as shown in Figure 3. The ground state in-plane orderings shown in Figure 3 are the same as those in the predicted ground states using LDA and optB88. All calculated hulls using LDA, optB88, and optB86 are compared in Supporting Information.

Voltage Profiles. The open-circuit voltage is related to the difference in Mg chemical potential between the cathode and the anode according to the Nernst equation:

$$V(x) = -[\mu_{Mg}(x) - \mu_{Mg}^{\text{reference}}]/2e$$

Here μ_{Mg} is the chemical potential of Mg in Mg_xTiS_2, and $\mu_{Mg}^{\text{reference}}$ is the chemical potential of Mg in a reference

DOI: 10.1021/acs.inorgchem.5b00188
Inorg. Chem. 2015, 54, 4394−4402

electrode. Here we use metallic Mg in the hcp crystal structure as the reference anode.

We calculated Mg chemical potentials at room temperature by applying Monte Carlo simulations to first-principles parametrized cluster expansions of the configurational energy of Mg-vacancy disorder in the O1 and spinel host structures. The cluster expansions were fit to the PBE-optB86-calculated formation energies. Grand-canonical Monte Carlo simulations were subsequently performed on the cluster expansions to calculate the dependence of the chemical potential on Mg concentration at room temperature, which was then inserted into the Nernst equation to obtain the voltage profile. Figure 4

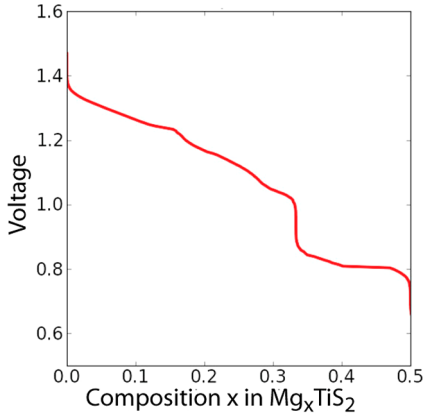

Figure 4. Voltage curve for O1 Mg_xTiS_2 calculated with Monte Carlo simulations at 300 K applied to a cluster expansion that was parametrized with PBE-optB86 energies.

shows the calculated voltage profile for O1 Mg_xTiS_2. The steps in the voltage profile are due to Mg-vacancy ordering at $x = {}^1/_6$, ${}^1/_3$, and ${}^1/_2$ (these orderings are shown in Figure 3), while the sloping regions at low and intermediate Mg concentration correspond to solid solutions characterized by Mg-vacancy disorder.

Contrary to the layered O1 material, spinel Mg_xTiS_2 exhibits more of a solid solution as x varies between 0 and 0.5 in Mg_xTiS_2 as is evident from the sloping voltage profile (Figure 5) across the entire composition range. This behavior is similar to spinel $LiTiS_2$.[42,43] Electrostatic interactions between Mg,

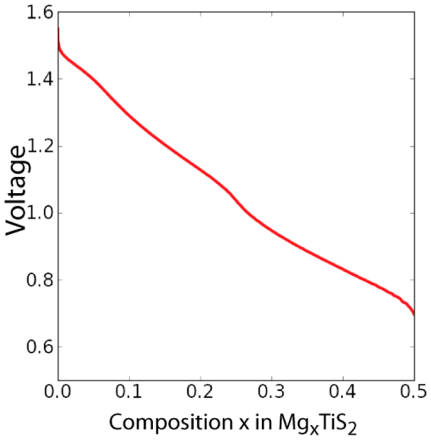

Figure 5. Spinel Mg_xTiS_2 voltage curve calculated with Monte Carlo simulations at 300 K applied to a cluster expansion that was parametrized with PBE-optB86 energies.

having a nominal valence of +2, are likely more screened in the three-dimensional spinel host compared to the layered O1 host, thereby decreasing an energetic tendency to order at intermediate concentrations.

Diffusion. We also explored diffusion in the spinel and O1 host structures. Similarly to layered and spinel Li_xTiS_2,[42,32] layered Li_xCoO_2,[34] and other layered transition metal oxides,[44] Mg ions in TiS_2 are predicted to migrate through a neighboring tetrahedral site where the energy exhibits a local minimum before moving to the adjacent octahedral site. However, the energy barriers for Mg^{2+} diffusion are substantially greater than those for Li^+ diffusion. Figure 6 shows a migration barrier at

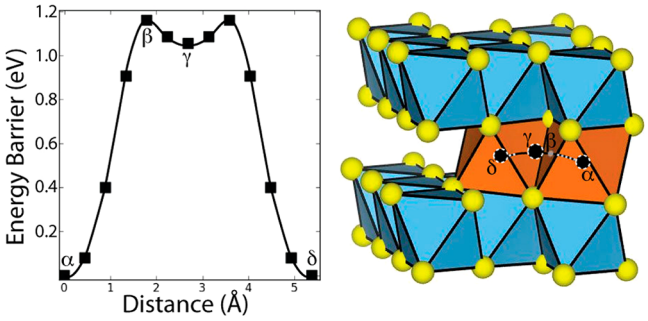

Figure 6. Migration barrier and pathway in dilute O1 $Mg_{1/32}TiS_2$. The pathway shows the motion of a Mg atom from an octahedral site (α) into an adjacent octahedral site (δ) through a tetrahedral site corresponding to a local minimum (γ). The maximum energy occurs when Mg passes through the trigonal face (β) shared by the octahedral and tetrahedral site.

dilute Mg concentrations as calculated in a 4 × 4 × 2 supercell of the primitive O1 structure, consisting of 32 TiS_2 formula units (i.e., composition $MgTi_{32}S_{64}$). The maximum barrier of 1.16 eV occurs when the Mg^{2+} passes through the face of a triangle created by three of the sulfur atoms of the MgS_6 octahedron (point β in Figure 6). The Mg−S distances along the migration path are the shortest at the center of the triangular face separating the tetrahedral and octahedral sites.

Because the c-lattice parameter can have a large effect on migration barriers,[32,34] we examined the sensitivity of the relative stability of the tetrahedral and octahedral sites in the O1 structure as a function of dimensional changes of the host. The difference in energy between tetrahedral versus octahedral Mg occupancy in the dilute limit was calculated in a 4 × 4 × 2 supercell of O1 TiS_2 for a range of c-lattice parameter values. One intercalation layer (Figure 3) was left completely empty, while the other layer contained a single magnesium atom. The Mg atom was initialized slightly off of the ideal octahedral site to allow for possible relaxations to a lower energy site to occur (e.g., preferentially shifting closer to one layer of sulfurs as opposed to staying at the center). Structures were distorted along the c-axis from 1% to 10%, allowing internal atomic relaxations while the cell shape remained fixed. Figure 7 shows energy differences between octahedral and tetrahedral sites in the O1 layered host structure. After relaxation, the layer with the Mg ion preferentially expands, while the empty layer contracts. The interslab spacing therefore increases when Mg migrates from the larger octahedral site to the smaller tetrahedral site, indicating that the migration barrier should be sensitive to the local state of strain. Figure 7 shows that the energy difference between tetrahedral versus octahedral

DOI: 10.1021/acs.inorgchem.5b00188
Inorg. Chem. 2015, 54, 4394−4402

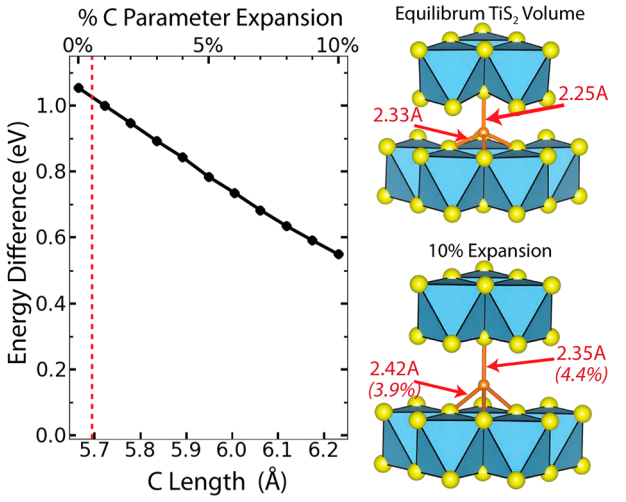

Figure 7. Energy differences between octahedral and tetrahedral sites in dilute O1 $MgTi_{32}S_{64}$. The dashed red line denotes the experimental *c*-lattice parameter for TiS_2 (5.7[7,39]), and bond lengths are shown for the PBE-optB86 relaxed lattice parameters of TiS2 and for a 10% increase of the *c*-lattice parameter. Percentage increases are shown in italicized parentheses for the 10% expansion figure.

occupancy decreases with increasing *c*-lattice parameter. This is similar to layered Li-intercalation compounds.[32,34]

In addition to exploring the relative stability between tetrahedral and octahedral sites, we also investigated how a variation in the *c*-lattice parameter affects the migration barrier between the two sites in dilute $Mg_{1/32}TiS_2$. Increasing the *c*-lattice parameter by 5% (shown in Figure 8) results in a

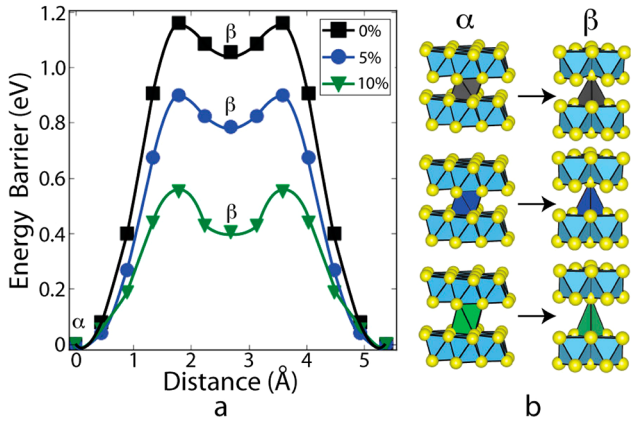

Figure 8. Effect of *c*-lattice parameter increases on the migration barrier in dilute O1 $Mg_{1/32}TiS_2$. Energy barriers are shown (a) for the equilibrium PBE + optB86 TiS_2 lattice parameters (black, top) and for a *c*-lattice parameter that is expanded by 5% (blue, middle) and 10% (green, bottom). (b) Schematics of bond length increases are shown with the same color scheme as that in part a.

decrease of the migration barrier from 1.16 to 0.90 eV. Further expansion of the *c*-axis by 10% results in an energy barrier of 0.55 eV. This points to a strong dependence of the migration barrier on the distance between the layers. The activated site is coordinated by three sulfur ions forming a triangle, and an increase in the area of this triangle results in a lowering of the migration barrier. This trend indicates that artificially increasing the distances between transition metal layers should result in higher Mg mobilities. Nevertheless, the barriers are probably not low enough to achieve sufficiently high diffusion coefficients at room temperature.

As the Mg concentration increases to $Mg_{1/3}TiS_2$, the structure expands slightly to accommodate the extra Mg. This results in a slight decrease in the migration barrier (Figure 9) for a Mg ion migrating from the initial octahedral site to an intermediate tetrahedral site.

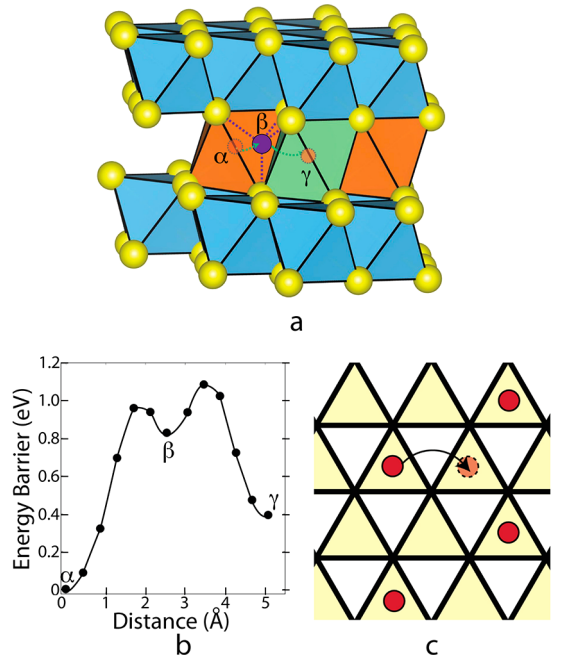

Figure 9. Mg hop in layered O1 $Mg_{1/3}TiS_2$. (a) Migration pathway from an octahedral site (α) to a local minimum at a tetrahedral site (purple, β) into an adjacent edge-sharing octahedron (γ, green). (b) Diffusion energy barrier and (c) hop path as projected along the *c*-axis into the plane of the intercalation layer.

However, due to the very stable $\sqrt{3}a \times \sqrt{3}a$ in-plane ordering in $Mg_{1/3}TiS_2$, any rearrangement of Mg due to diffusion will result in an increase in the energy of the end states of the hop as shown in Figure 9b. It is well-known that self-diffusion coefficients can drop dramatically at stoichiometric compositions corresponding to stable ordered phases.[34] Often, though, this drop in the self-diffusion coefficient is compensated by a rapid increase with concentration of the thermodynamic factor, minimizing the effect of ordering on the chemical diffusion coefficient appearing in Fick's first law of diffusion.[34]

Similar behavior is predicted in the $Mg_{1/2}TiS_2$ ground state ordering as shown in Figure 10. A hop involving a Mg within one of the ordered rows is accompanied by an increase of the energy of the end state of the hop (Figure 9b), as this end state disrupts the energetically stable ordering. Nevertheless, the overall migration barrier is lower than that at more dilute Mg concentrations, in part due to an increase in the *c*-lattice parameter with Mg concentration.

The Mg-migration barriers in the spinel host in the dilute limit are substantially lower than those in the layered form at dilute concentrations. The barrier for a Mg hop from an octahedral site to a tetrahedral site is 0.86 eV at the equilibrium spinel TiS_2 lattice parameters. These barriers were calculated in the $2 \times 2 \times 2$ supercell of the primitive spinel crystal structure (with the composition $MgTi_{32}S_{64}$). Figure 11 illustrates the

DOI: 10.1021/acs.inorgchem.5b00188
Inorg. Chem. 2015, 54, 4394−4402

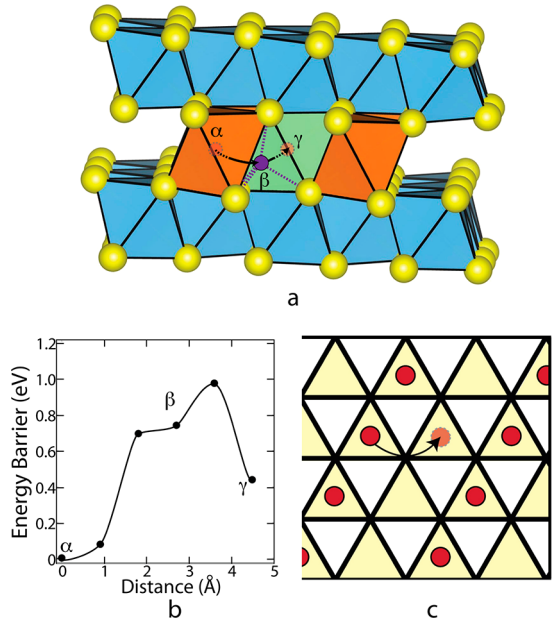

Figure 10. Mg hop in layered O1 $Mg_{1/2}TiS_2$. (a) Migration pathway from an octahedral site (α) through a trigonal planar face to a local minimum at a tetrahedral site (purple, β) into an adjacent edge-sharing octahedron (γ, green). (b) Diffusion energy barrier and (c) hop path as projected along the c-axis into the plane of the intercalation layer.

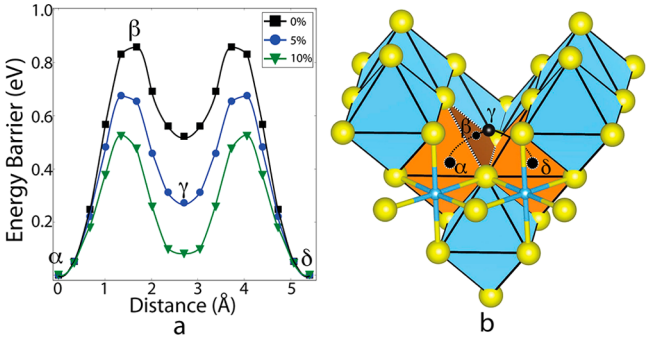

Figure 11. Mg hop in dilute spinel $Mg_{1/32}TiS_2$. (a) Migration barrier for the equilibrium PBE-optB86 volume (black squares) of spinel TiS_2 (a = 9.69 Å), for a volume expanded by 5% (blue circles) and for a volume expanded by 10% (green triangles). (b) Mg hop path between a pair of octahedral sites in spinel TiS_2.

pathway at dilute Mg concentrations. Like the layered compound, the tetrahedral site is a local minimum. In fact, the tetrahedral site resides in a deeper energy well in the spinel host structure than in the O1 host.

We also examined the dependence of the energy differences between octahedral and tetrahedral sites on the volume of the spinel crystal structure. These calculations were performed for a single Mg in a 2 × 2 × 2 supercell of the primitive spinel crystal (with the composition $MgTi_{32}S_{64}$), incrementally increasing the volume by 10% and allowing for internal atomic relaxations at each volume. These results are shown in Figure 12. A nudged elastic band calculation at a 5% increase in volume predicts a decrease in the overall migration barrier by ~0.2 eV, to 0.68 eV, shown in Figure 11a. These barriers, however, are too high to ensure mobilities comparable to Li-intercalation compounds at room temperature.

Charge Distribution. The insertion of a cation into an intercalation compound results in some degree of rehybridization between the transition metals and anions of the host.[46] In Li_xCoO_2, for example, an increase in Li concentration progressively increases the ionic character of the cobalt–oxygen bonds due to a reduction in the hybridization between Co d states and oxygen p states as the electron from Li is donated to the host.[35,47] Mg donates two electrons to the host and thereby induces more rehybridization between the cation and the anion than occurs with Li intercalation. In this section, we explore the degree of rehybridization between Mg and Li insertion into both the layered and spinel crystal structures and how it may affect the migration barrier for diffusion.

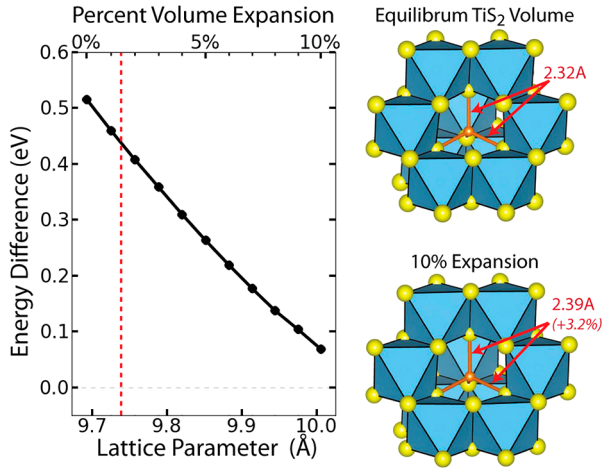

Figure 12. Effect of a volume increase on the difference in energy between tetrahedral versus octahedral occupancy by Mg in spinel $MgTi_{32}S_{64}$. The dashed red line shows the experimental lattice parameter at 9.737 Å[45] of spinel TiS_2. Bond lengths are shown for the relaxed structures for the PBE-optB86 TiS_2 parameters and for lattice parameters corresponding to a 10% increase in volume.

In TiS_2, bonding between Ti and S has substantial covalent character. The Ti cations reside in the octahedral sites of the close-packed sulfur sublattice. The ligand field of the negatively charged sulfur anions splits the degeneracy of the Ti 3d orbitals: the $d_{3x^2-y^2}$ and $d_{z^2-r^2}$ orbitals, with lobes pointing directly toward the negatively charged sulfur anions, are raised in energy, while the d_{xy}, d_{xz}, and d_{yz} orbitals with lobes pointing between sulfur anions are less affected. In addition to a ligand field splitting, there is also covalent hybridization between Ti and S, with σ bonds forming between sulfur p states and Ti $d_{3z^2-r^2}$, $d_{x^2-y^2}$, 4s, and 4p states.

The degree of covalency of the σ bonds between the sulfur p states and the Ti $d_{3z^2-r^2}$ and $d_{x^2-y^2}$ orbitals changes upon insertion of Li or Mg to the TiS_2 host. The electrons accompanying Li or Mg are donated to the host and fill the lower nonbonding Ti d_{xy}, d_{xz}, and d_{yz} orbitals that point between the sulfur anions. The increased negative charge around the Ti ions in turn raises the energy of the d states relative to that of the sulfur p states, causing a reduction in covalency and an increase in polarization of the σ bond made of the Ti $d_{3z^2-r^2}$ and $d_{x^2-y^2}$ orbitals and the sulfur p orbitals. The shift from covalent bonding to more ionic bonding between Ti and S increases the charge around the sulfur anions.[46] The sulfur anions most affected are those directly coordinating the inserted Mg or Li cation, whose effective positive valence polarizes the negative charge toward it.

Figure 13 shows charge difference plots as Mg (Li) is inserted in an octahedral site and a tetrahedral site of the O1 form of TiS_2. These charge difference plots were obtained by

DOI: 10.1021/acs.inorgchem.5b00188
Inorg. Chem. 2015, 54, 4394–4402

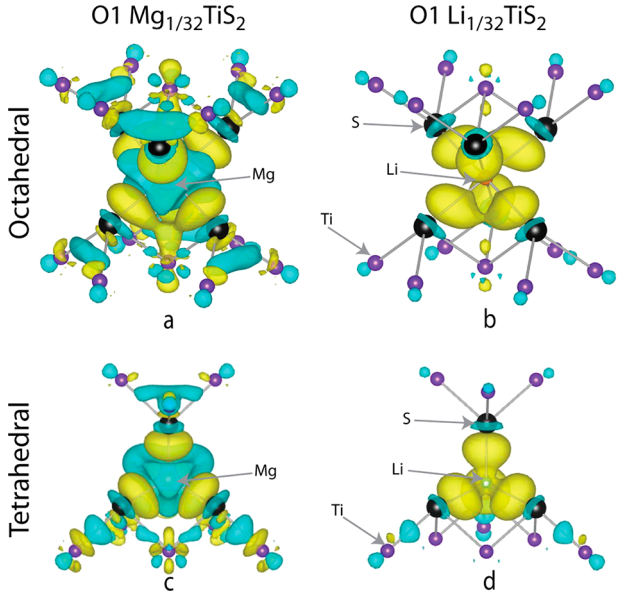

Figure 13. Charge difference plots of layered TiS_2 having the O1 crystal structure with an isolated Mg (a) in a tetrahedral site and (c) in an octahedral site, and with an isolated Li (b) in a tetrahedral site and (d) in an octahedral site (d). Blue regions denote areas of charge depletion while yellow regions denote charge accumulation. Black balls are sulfur, and purple balls are Ti.

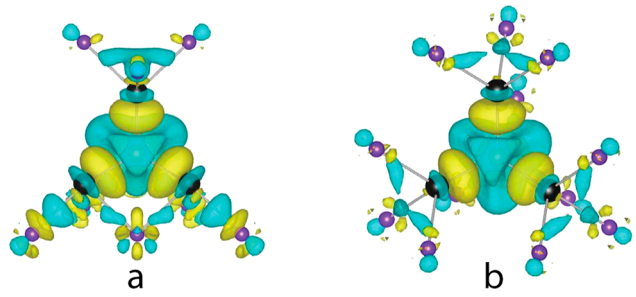

Figure 14. Charge rehybridization upon insertion of a Mg in the tetrahedral site of (a) layered O1 and (b) spinel TiS_2 with identical S−S bond lengths. Areas of charge accumulation are shown in yellow while depletion is shown in blue. Sulfur atoms are shown as large black spheres, Ti as small purple spheres, and Mg at the center as an orange sphere. Bonds are drawn in gray. All surrounding atoms with negligible charge rehybridization have been hidden for clarity. The spinel structure has 12 Ti atoms participating in charge rehybridization located in four groups of three Ti atoms, while the O1 structure has 9 Ti atoms participating in charge rehybridization, with one group of three shown at the top of part a and the remaining six clustered in a network at the bottom of a.

subtracting the charge densities of both TiS_2 structures and an isolated Mg or Li atom from the charge density of Mg_xTiS_2 and Li_xTiS_2 for crystal structures in which Ti and S are at identical positions. The charge difference plots therefore show how charge redistributes upon addition of Li or Mg to TiS_2. Yellow signifies an accumulation while blue signifies a depletion of electron density. As is clear for both Mg and Li insertion, there is substantial charge polarization toward the inserted cation. The rehybridization of the Ti d orbitals is also clearly evident. The d orbitals pointing along the Ti−S bond toward the sulfur coordinating the inserted Mg or Li undergo a depletion of electron density, resulting in less overlap between Ti d orbitals and S p orbitals. Simultaneously, nonbonding d orbitals (i.e., a combination of d_{xy}, d_{xz}, and d_{yz}) that point between S ions accumulate charge density. As is clear in Figure 13, the rehybdridization around Ti upon Mg insertion is substantially larger than that resulting from Li insertion due to the introduction to the host structure of two electrons per Mg as opposed to one for Li.

As a Mg or Li ion migrates through the crystal, it will drag its electron cloud residing on the coordinating sulfur anions with it. The surrounding Ti and sulfur cations will therefore be required to rehybridize as the cation moves. Figure 13 shows that the rehybridization around Ti is more concentrated over fewer bonds when Mg or Li resides in the tetrahedral site versus the octahedral site. This is due to the lower S coordination of the tetrahedral site compared to the octahedral site.

Figure 14 compares charge difference plots for Mg insertion into tetrahedral sites of O1 and spinel TiS_2. While the O1 and spinel hosts both consist of close-packed anion sublattices, the different arrangements of the Ti ions over the octahedral sites result in differing degrees of rehybridization. The charge difference plots of Figure 14 were calculated using identical Ti−S and S−S nearest neighbor bond lengths in the O1 and spinel hosts. This allows us to isolate the role of Ti ordering on rehybridization in the tetrahedral site from contributions due to differences in local relaxations. As is clear in Figure 14, the rehybridization in the spinel tetrahedral sites is more evenly distributed than that in the tetrahedral site of layered O1. In spinel, each S anion coordinating a tetrahedral Mg site hybridizes with three Ti. In layered O1, only one of the four S anions coordinating a tetrahedral site hybridizes evenly with three Ti (the top sulfur atom in Figure 14a), while the remaining three S hybridize primarily with only one Ti each and partially hybridize with two additional Ti that are "shared" by the other S anions. The rehybridization per Ti−S bond upon Mg insertion into a tetrahedral site is therefore more pronounced in the layered host than in spinel.

DISCUSSION

In this work, we have studied the thermodynamic, kinetic, and electronic properties of $MgTiS_2$ in common intercalation compound crystal structures. Thermodynamically, Mg_xTiS_2 and Li_xTiS_2 are stable in similar structures. For both, the spinel structure is metastable, and the layered O1 compound is energetically preferred at all compositions. Mg and Li also prefer the octahedral sites to the tetrahedral sites in both forms of TiS_2. The voltage profiles for both Li and Mg insertion into the two TiS_2 hosts are also qualitatively similar, although Mg intercalation results in more stable intermediate ordered phases than Li intercalation,[32,42] as manifested by steps in the voltage profile. The increased stability of Mg-vacancy ordering at room temperature as compared to similar Li-vacancy ordering within TiS_2 is likely due to larger electrostatic interactions between Mg^{2+} ions. Since Li^+ and Mg^{2+} have similar ionic radii, the relaxations of the host around Li or Mg due to steric factors should be similar.

The mobilities of Mg and Li in both O1 and spinel TiS_2 differ substantially. Although Li and Mg are predicted to hop with the same mechanism, passing through an intermediate tetrahedral site, the Mg mobility within the TiS_2 host structures is significantly lower than that of Li due to much larger migration barriers (Figures 5 and 7−10). The Mg diffusion coefficients in TiS_2 will therefore have quantitative values that are more typical of substitutional diffusion[48] in alloys than that

DOI: 10.1021/acs.inorgchem.5b00188
Inorg. Chem. 2015, 54, 4394−4402

of interstitial diffusion.[32,34,42,44,49] As with Li diffusion,[32,34,44] the migration barrier for Mg diffusion is very sensitive to the lattice parameter c of the O1 host and to the volume of the spinel host, as shown in Figures 7 and 8 and Figures 11 and 12, respectively.

The migration barriers for both Li and Mg hops between octahedral sites in layered O1 and spinel TiS_2 correlate with the difference in energy between octahedral site and tetrahedral site occupancy. Several factors that contribute to the difference in site energies between tetrahedral and octahedral sites can be identified. One is the size of the site and the flexibility of coordinating ions of the particular host crystal structure to relax once occupied by an intercalating species. Another is the electrostatic energy, which may be more favorable in one interstitial site relative to the other. There are also more complex quantum mechanical effects including the flexibility of adjacent ions to rehybridize as the positively charged cation migrates from one site to another.

There are no unambiguous ways to disentangle the role of purely electrostatic interactions from the quantum mechanical interactions responsible for rehybridization. Nevertheless, the charge difference plots comparing charge redistribution upon Mg insertion into tetrahedral sites (Figure 14) show that the degree of rehybridization per Ti−S bond is more pronounced in O1 than in spinel TiS_2. This is due to the lower coordination of the tetrahedral S anions by Ti in the O1 host compared to the spinel host. The lower migration barrier in spinel compared to that in O1 also suggests that a higher coordination of the anion sublattice with transition metal cations is likely to reduce the migration barrier as it distributes the rehybridization over more metal−anion bonds. These features are present in the Mo_6X_8 (X = S, Se) Chevrel phases exhibiting reasonable Mg mobilities, where the transition metal to anion ratio is higher than that in most intercalation compounds. Lower migration barriers may also be achievable using transition metal ions that readily shift by more than one valence state, such as Mo, as they are likely to be more flexible in rehybridizing as Mg migrates through the crystal.

CONCLUSIONS

Using first-principles and statistical mechanics tools, we systematically investigated Mg_xTiS_2 and compared it to its well-studied Li counterpart, Li_xTiS_2. We find that Mg in both the layered and spinel forms of TiS_2 occupies the same sites as Li ions in Li_xTiS_2 (i.e., the octahedrally coordinated interstitial sites). Furthermore, Mg intercalation into the layered form of TiS_2 does not induce changes in the stacking sequence of the TiS_2 slabs. Predicted voltage profiles are similar to those of $LiTiS_2$, but show pronounced steps due to strong thermodynamic tendencies for Mg-vacancy ordering over the octahedral sites. We also find that the Mg-diffusion mechanisms are identical to those of Li in layered and spinel TiS_2, whereby the migration between neighboring octahedral sites involves the passage through an intermediate tetrahedral site. Nevertheless, contrary to Li diffusion in $LiTiS_2$,[42,32] Mg mobility is very sluggish at room temperature, with typical migration barriers predicted to be on the order of ∼1 eV. With the consideration that the sulfides exhibit among the most facile Li-insertion and -removal kinetics of all layered intercalation compounds (including the oxides), this result suggests that popular intercalation host chemistries and crystal structures for Li-ion batteries are unlikely to be suited for Mg intercalation at room temperature. An analysis of the dependence of Mg-migration barriers on dimensional changes of the host, however, indicates that the size of the migration channel between adjacent sites is an important factor in determining migration barriers. Designing intercalation compounds in ways that lead to an increased separation of the slabs, by, for example, inserting dilute concentrations of large and immobile cations or molecules in the intercalation layers, may lead to higher Mg mobilities. Electronic effects are also likely to play an important role since the rehybridization between transition metal and anion is more severe upon Mg insertion than upon Li insertion. Transition metals that are more flexible in shifting valence and that thereby can more easily rehybridize as Mg migrates through the crystal should help to reduce migration barriers.

ASSOCIATED CONTENT

Supporting Information

Calculated convex hulls for Mg_xTiS_2 ($0 < x < 0.5$) using LDA and PBE-vdW-DF methods. Octahedral and tetrahedral site energy differences in dilute $MgTi_{32}S_{64}$ using LDA and PBE-vdW-DF methods. Calculated voltage curves with Monte Carlo simulations applied to cluster expansion parametrized using LDA and PBE-vdW-DF energy calculations. This material is available free of charge via the Internet at http://pubs.acs.org.

AUTHOR INFORMATION

Corresponding Author

*E-mail: avdv@engineering.ucsb.edu.

Notes

The authors declare no competing financial interest.

ACKNOWLEDGMENTS

A.E. thanks Manos Kioupakis for useful discussion regarding charge distribution as well as Guangsha Shi for assistance in determining isosurface levels. This material is based upon work supported by the National Science Foundation, Grant DMR-1410242. Computational resources provided by the National Energy Research Scientific Computing Center (NERSC), supported by the Office of Science and U.S. Department of Energy, under Contract DE-AC02-05CH11231, are also gratefully acknowledged. Images of crystal structures were produced with VESTA.[50]

REFERENCES

(1) Guo, Y.; Yang, J.; NuLi, Y.; Wang, J. *Electrochem. Commun.* **2010**, *12*, 1671−1673.
(2) Matsui, M. *J. Power Sources* **2011**, *196*, 7048−7055.
(3) Bruce, P. G.; Krok, F.; Nowinski, J.; Gibson, V. C.; Tavakkoli, K. *J. Mater. Chem.* **1991**, *1*, 705.
(4) Pereira-Ramos, J. P.; Messina, R.; Perichon, J. *J. Electroanal. Chem. Interfacial Electrochem.* **1987**, *218*, 241−249.
(5) Novák, P.; Scheifele, W.; Haas, O. *J. Power Sources* **1995**, *54*, 479−482.
(6) Le, D. B.; Passerini, S.; Coustier, F.; Guo, J.; Soderstrom, T.; Owens, B. B.; Smyrl, W. H. *Chem. Mater.* **1998**, *10*, 682−684.
(7) Whittingham, M. S. *J. Electrochem. Soc.* **1976**, *123*, 315.
(8) Whittingham, M. S. *Prog. Solid State Chem.* **1978**, *12*, 41−99.
(9) Whittingham, M. S. *Chem. Rev.* **2004**, *104*, 4271−4302.
(10) Saha, P.; Datta, M. K.; Velikokhatnyi, O. I.; Manivannan, A.; Alman, D.; Kumta, P. N. *Prog. Mater. Sci.* **2014**, *66*, 1−86.
(11) Yoo, H. D.; Shterenberg, I.; Gofer, Y.; Gershinsky, G.; Pour, N.; Aurbach, D. *Energy Environ. Sci.* **2013**, *6*, 2265.
(12) Muldoon, J.; Bucur, C. B.; Oliver, A. G.; Sugimoto, T.; Matsui, M.; Kim, H. S.; Allred, G. D.; Zajicek, J.; Kotani, Y. *Energy Environ. Sci.* **2012**, *5*, 5941.

DOI: 10.1021/acs.inorgchem.5b00188
Inorg. Chem. 2015, 54, 4394−4402

(13) Doe, R. E.; Han, R.; Hwang, J.; Gmitter, A. J.; Shterenberg, I.; Yoo, H. D.; Pour, N.; Aurbach, D. *Chem. Commun.* **2014**, *50*, 243−245.
(14) Tao, Z.-L.; Xu, L.-N.; Gou, X.-L.; Chen, J.; Yuan, H.-T. *Chem. Commun.* **2004**, 2080−2081.
(15) Novák, P.; Imhof, R.; Haas, O. *Electrochim. Acta* **1999**, *45*, 351−367.
(16) Novák, P. *J. Electrochem. Soc.* **1993**, *140*, 140.
(17) Ichitsubo, T.; Adachi, T.; Yagi, S.; Doi, T. *J. Mater. Chem.* **2011**, *21*, 11764.
(18) Ling, C.; Banerjee, D.; Song, W.; Zhang, M.; Matsui, M. *J. Mater. Chem.* **2012**, *22*, 13517.
(19) Ling, C.; Mizuno, F. *Chem. Mater.* **2013**, *25*, 3062−3071.
(20) Levi, E.; Gershinsky, G.; Aurbach, D.; Isnard, O.; Ceder, G. *Chem. Mater.* **2009**, *21*, 1390−1399.
(21) Levi, E.; Levi, M. D.; Chasid, O.; Aurbach, D. *J. Electroceram.* **2007**, *22*, 13−19.
(22) Thackeray, M. M. *Prog. Solid State Chem.* **1997**, *25*, 1−71.
(23) Zhou, F.; Maxisch, T.; Ceder, G. *Phys. Rev. Lett.* **2006**, *97*, 155704.
(24) Kresse, G. *Phys. Rev. B* **1996**, *54*, 11169−11186.
(25) Kresse, G.; Furthmüller, J. *Comput. Mater. Sci.* **1996**, *6*, 15−50.
(26) Kresse, G. *Phys. Rev. B* **1999**, *59*, 1758−1775.
(27) Blöchl, P. E. *Phys. Rev. B* **1994**, *50*, 17953−17979.
(28) Klimeš, J.; Bowler, D. R.; Michaelides, A. *Phys. Rev. B* **2011**, *83*, 195131.
(29) Klimeš, J.; Bowler, D. R.; Michaelides, A. *J. Phys.: Condens. Matter* **2010**, *22*, 022201.
(30) Mills, G.; Jónsson, H.; Schenter, G. K. *Surf. Sci.* **1995**, *324*, 305−337.
(31) Sanchez, J. M.; Ducastelle, F.; Gratias, D. *Phys. A* **1984**, *128*, 334−350.
(32) Van der Ven, A.; Thomas, J.; Xu, Q.; Swoboda, B.; Morgan, D. *Phys. Rev. B* **2008**, *78*, 104306.
(33) Puchala, B.; Van der Ven, A. *Phys. Rev. B* **2013**, *88*, 094108.
(34) Van der Ven, A.; Ceder, G.; Asta, M.; Tepesch, P. *Phys. Rev. B* **2001**, *64*, 184307.
(35) Van der Ven, A.; Aydinol, M. K.; Ceder, G.; Kresse, G.; Hafner, J. *Phys. Rev. B* **1998**, *58*, 2975.
(36) Chevrier, V. L.; Ong, S. P.; Armiento, R.; Chan, M. K. Y.; Ceder, G. *Phys. Rev. B* **2010**, *82*, 075122.
(37) Delmas, C.; Fouassier, C.; Hagenmuller, P. *Physica B+C* **1980**, *99*, 81−85.
(38) Safran, S. A. *Solid State Phys.* **1987**, *40*, 183−246.
(39) Dahn, J. R.; Haering, R. R. *Solid State Commun.* **1981**, *40*, 245−248.
(40) Van der Ven, A.; Aydinol, M.; Ceder, G. *J. Electrochem. Soc.* **1998**, *145*, 2149.
(41) Chen, Z.; Lu, Z.; Dahn, J. R. *J. Electrochem. Soc.* **2002**, *149*, A1604.
(42) Bhattacharya, J.; Van der Ven, A. *Phys. Rev. B* **2011**, *83*, 144302.
(43) Sinha, S.; Murphy, D. *Solid State Ionics* **1986**, *20*, 81−84.
(44) Van der Ven, A.; Bhattacharya, J.; Belak, A. A. *Acc. Chem. Res.* **2013**, *46*, 1216−1225.
(45) Bodenez, V.; Dupont, L.; Morcrette, M.; Surcin, C.; Murphy, D. W.; Tarascon, J.-M. *Chem. Mater.* **2006**, *18*, 4278−4287.
(46) Aydinol, M.; Kohan, A.; Ceder, G.; Cho, K.; Joannopoulos, J. *Phys. Rev. B* **1997**, *56*, 1354−1365.
(47) Wolverton, C.; Zunger, A. *Phys. Rev. Lett.* **1998**, *81*, 606−609.
(48) Van der Ven, A.; Yu, H.; Ceder, G.; Thornton, K. *Prog. Mater. Sci.* **2010**, *55*, 61.
(49) Bhattacharya, J.; Van der Ven, A. *Phys. Rev. B* **2010**, *81*, 104304.
(50) Momma, K.; Izumi, F. *J. Appl. Crystallogr.* **2011**, *44*, 1272−1276.

DOI: 10.1021/acs.inorgchem.5b00188
Inorg. Chem. 2015, 54, 4394−4402